Coastal Engineering 58 (2011) 429–443

Contents lists available at ScienceDirect

Coastal Engineering

journal homepage: www.elsevier.com/locate/coastaleng

Wave refraction–diffraction effect in the wind wave model WWM

Jian-Ming Liau [a], Aaron Roland [b], Tai-Wen Hsu [c,*], Shan-Hwei Ou [d], Yi-Ting Li [e]

[a] Taiwan Ocean Research Institute, National Applied Research Laboratories, Kaohsiung 852, Taiwan
[b] Institute for Hydraulic and Water Resources Engineering, Technische Universität Darmstadt, Rundeturmstr. 1, Darmstadt 60483, Germany
[c] Department of Hydraulic and Ocean Engineering, National Cheng Kung University, Tainan 701, Taiwan
[d] Department of Environmental Resources Management, Tajen University, Pingtung 907, Taiwan
[e] Institute of Ocean Technology and Marine Affairs, National Cheng Kung University, Tainan 701, Taiwan

ARTICLE INFO

Article history:
Received 27 July 2010
Received in revised form 23 December 2010
Accepted 4 January 2011
Available online 1 February 2011

Keywords:
Wave refraction–diffraction
Wave reflection
Phase-decoupled wave model
Higher-order bottom components
Wave–current interaction

ABSTRACT

Based on the extended mild-slope equation, the wind wave model (WWM; Hsu et al., 2005) is modified to account for wave refraction, diffraction and reflection for wind waves propagating over a rapidly varying seabed in the presence of current. The combined effect of the higher-order bottom effect terms is incorporated into the wave action balance equation through the correction of the wavenumber and propagation velocities using a refraction–diffraction correction parameter. The relative importance of additional terms including higher-order bottom components, the wave–bottom interaction source term and wave–current interaction that influence the refraction–diffraction correction parameter is discussed. The applicability of the proposed model to calculate a wave transformation over an elliptic shoal, a series of parallel submerged breakwater induced Bragg scattering and wave–current interaction is evaluated. Numerical results show that the present model provides better predictions of the wave amplitude as compared with the phase-decoupled model of Holthuijsen et al. (2003).

1. Introduction

The combined effect of the wave refraction, diffraction and reflection on the wave transformation can be accounted for by using the mild-slope equation (MSE) which was first derived by Berkhoff (1972). The MSE is a phase-resolving wave model to describe wave transformations from deep water to shallow water depth in a slowly varying sea bottom. Many studies have been performed to extend the MSE to describe the wave propagating over a rapidly varying seabed (e.g. Kirby, 1986; Massel, 1993; Chamberlain and Porter, 1995a, 1995b; Hsu and Wen, 2001a, 2001b; Liu, 1990). The influence of the ambient current on the MSE using Luke's variation principle was given by Kirby (1984) and Dingemans (1985). All quantities of the wavenumber k, the absolute frequency ω and the intrinsic frequency σ are determined for a linear wave–current interaction system with the help of the dispersion relation $\sigma^2 = gk \tanh kh$, the Doppler-shift relation $\omega = \sigma + \boldsymbol{k} \cdot \boldsymbol{U}$, and the condition of irrotationality of the wavenumber vector $\nabla_h \times \boldsymbol{k} = 0$, where $\nabla_h = (\partial/\partial x, \partial/\partial y)$ is the horizontal gradient operator, k the wavenumber vector and U the current vector.

Boussinesq equations (BES) are the other types of phase-resolving models to account for nearshore wave processes in which nonlinearity and frequency dispersion are included. The classical BES of Peregrine (1967) poorly described the frequency dispersion and nonlinearity in the intermediate water depth. The dispersion property of the classical BES was improved by modifying the dispersion terms (Madsen and Sørensen, 1992) or applying a reference velocity at a specified depth (Nwogu, 1993). The improved BES enhanced the conventional one to an equivalence of a Padé approximation of the linear dispersion relation. Wei et al. (1995) presented a set of highly nonlinear BES and Gobbi et al. (2000) derived a fully nonlinear approach with the fourth order. Further improvements by introducing higher-order nonlinearity were also provided by Madsen et al. (2003) and Fuhrman and Madsen (2009). All of these efforts successfully extended the usefulness of BES to accurately simulate waves propagating from deep water to shallow water.

For practical applications, semi-empirical approaches were developed to account for wave breaking and energy dissipation with the prescribed criteria for the onset of wave breaking and incorporated additional terms in the MSE (Isobe, 1987; Tsai et al., 2001; Hsu and Wen, 2001b) and BES (Zelt, 1991; Wei et al., 1995; Lynett et al., 2002). The real sea state is notably random, both the MSE and BES are able to account for the feature of nonlinear waves, irregular random waves and transient waves in the time-domain. However, from the physical point of view, they are limited in representing the evolution of the wave spectrum such as the relative importance of the nonlinear transfer, the exact source function expression of the wave growth and decay and their statistical description. As addressed by Holthuijsen et al. (2003), adding refraction–diffraction to a spectral model has some advantages such as that large-scale computations remain

* Corresponding author. Tel.: +886 6 2372315; fax: +886 6 2741463.
E-mail address: twhsu@mail.ncku.edu.tw (T.-W. Hsu).

0378-3839/$ – see front matter. Crown Copyright © 2011 Published by Elsevier B.V. All rights reserved.
doi:10.1016/j.coastaleng.2011.01.002

flexible, the characteristics of random short-crested waves is retained, and all physical processes as mentioned above are included.

The other phase-averaged models, such as SWAN (Simulating Wave Nearshore)(Booij et al., 1999; Ris et al., 1999), STWAVE (Steady-state spectral WAVE model) (Smith et al., 2001), TOMOWAC (Marcos, 2003) and WWM (Wind Wave Model)(Hsu et al., 2005) were developed to compute the variation of the wave spectra for random short-crested waves in large-scale oceanic deep water and small-scale shallow water regions. Although the effect of refraction is readily accounted for, wave diffraction is still not well implemented in these models. The approach by adding a diffraction to a spectral model with spatial or spectral diffusion was suggested by Resio (1988), Booij et al. (1997) and Mase (2001). The model is limited in the simulation of the diffraction induced turning of the wave direction.

Booij et al. (1997) and Rivero et al. (1997) tried to add wave diffraction to spectral models in which the diffraction effect is included in the propagation velocities through the modified wavenumber obtained from an energy balance equation of the MSE. Mase (2001) argued that their resulting models seem to be unstable in their numerical calculations due to the higher-order derivatives of the wave amplitude with respect to spatial coordinate, and thus developed a simple and robust spectral model based on an energy balance equation combined with an energy dissipation term and a diffraction-correction term. Holthuijsen et al. (2003) proposed an alternative in which a combination of two different wave models is implemented to add wave diffraction obtained from the MSE to the spectral model SWAN. The method is referred to as the phase-decoupled wave model. This phase-decoupled model still retains all the physical processes of energy generation, dissipation and wave–wave interactions and the specific feature of random waves is inherent. The model has been validated in some diffraction-prone cases in which verifications were made in small-scale conditions with random, shorted-crested waves., that are more than in the intended range of applications.

Holthijsen et al.'s model was also employed to calculate the multidirectional wave transformation around the detached breakwater by Ilic et al. (2007). The performance of wave diffraction in the model was examined for different incident wave conditions of wind–sea, swell–sea and bimodal spectra. The excellent agreement was found through comparisons of model predictions and field observations for broad frequency and directional spectra. The sensitivity tests were also conducted for the spatial resolution of the computational mesh and the filtering of the calculation of the wave refraction, diffraction and reflection correction parameter.

However, the MSE used in the formulation of Holthuijsen et al. (2003) is obtained by assuming a linear theory of surface gravity waves over a mildly sloping bottom. In a coastal region, offshore reefs and bars are usually present on the seabed, and the bottom configuration is generally arbitrary and extremely complicated. Furthermore, there usually exists an ambient current field in the sea due to wind shear stress or gradient of driving forces such as the wind shear stresses, attractive, coriolis, hydrostatic forces and so on. This is also not accounted for in the MSE applied by Holthuijsen et al. (2003). It is thus desirable to extend Holthuijsen et al.'s refraction–diffraction phase-decoupled wave model to a more realistic condition. Based on the Ardhuin and Herbers' (2002) method, wave reflection is also included in the model.

In this paper, the MSE including the higher-order bottom slope terms and ambient current effects is introduced into the wave action balance equation. The phase-averaged wave action equation is formulated to include refraction and diffraction-induced directional tuning rate of the components. The approximation is thus implemented into the WWM, which has been coded with the finite element method (FEM) by Hsu et al. (2005). The extension of wave refraction, diffraction and reflection in the WWM could give more accurate results and can be applied in most situations with rapidly varying topography where wave diffraction is dominant such as in the lee of islands and breakwater. The relative importance of the higher-order terms of the steep slopes, curvatures and wave–current interactions that influence the wave diffraction are evaluated in this study. Several computational cases with wave travelling over an abruptly varying topography or in current fields were performed to validate the proposed model.

2. Higher-order MSE with current effect

Considering the second-order bottom effects, bottom curvature $\nabla_h^2 h$ and bottom slope $|\nabla_h h|$, as well as the influence of the ambient current fields, the EMSE (extended mild-slope equation) is thus given by (Liu, 1990)

$$\begin{aligned}\nabla_h\cdot\left(cc_g\nabla_h\phi\right)+k^2cc_g\phi+\left(f_1g\nabla_h^2h+f_2gk|\nabla_hh|^2\right)\phi\\+i\omega[\boldsymbol{U}\cdot\nabla_h\phi+\nabla_h\cdot(\boldsymbol{U}\phi)]-\left(\sigma^2-\omega^2\right)\phi\\=\nabla_h\cdot[\boldsymbol{U}(\boldsymbol{U}\cdot\nabla_h\phi)]\end{aligned} \tag{1}$$

where

$$f_1=\frac{-4kh\,\cosh kh+\sinh 3kh+\sinh kh+8(kh)^2\sinh kh}{8\cosh^3 kh(2kh+\sinh 2kh)}-\frac{kh\tanh kh}{2\cosh^2 kh} \tag{2}$$

$$\begin{aligned}f_2=&\frac{\mathrm{sech}^2kh\left[8(kh)^4+16(kh)^3\sinh 2kh-9\sinh^2kh\cosh 2kh\right]}{6(2kh+\sinh 2kh)^3}\\&+\frac{12(kh)\left(1+2\sinh^4kh\right)(kh+\sinh 2kh)}{6(2kh+\sinh 2kh)^3}\end{aligned} \tag{3}$$

$\phi=\phi(x,y)=\frac{iga(x,y)}{\sigma}\frac{\cosh k(z+h)}{\cosh kh}e^{is(x,y)}$ is the velocity potential, $a(x,y)$ the wave amplitude, $S(x,y)$ the phase function, c and c_g the phase and group velocities, respectively, $i=\sqrt{-1}$ the unit complex number, g the gravitational acceleration and h the mean water depth. The detailed derivation of Eq. (1) can be found in Liu (1990).

Upon substituting the expression for the velocity potential into Eq. (1) and taking the real part, we obtain the resulting eikonal equation due to the wave diffraction effect:

$$\begin{aligned}K^2&=|\nabla_hS|^2\\&=k^2+\frac{\nabla_h\cdot\left(cc_g\nabla_ha\right)}{cc_ga}+\frac{f_1g\nabla_h^2h+f_2gk|\nabla_hh|^2}{cc_g}\\&\quad+\frac{1}{cc_g}\left\{-\sigma^2+(\omega-U\cdot\nabla_hS)^2-\frac{1}{a}\nabla_h\cdot[U(U\cdot\nabla_ha)]\right\}\end{aligned} \tag{4}$$

where K is the wavenumber caused by the combined effect of the wave amplitude, bottom configuration and current field. It should be noted that $K=|\mathbf{K}|$ is instead of $k=|\mathbf{k}|$ to emphasize the difference between $\mathbf{K}$ and $\mathbf{k}$ due to the wave diffraction effect. The derivation of Eq. (4) is given in Appendix A.

The Doppler-shift relation between the absolute and intrinsic frequencies for the linear wave–current coexisting system is given by

$$\omega=\sigma+k\cdot U=\sigma+kU_x\cos\theta+kU_y\sin\theta=\sigma+kU_s \tag{5}$$

where $U_s=U_x\cos\theta+U_y\sin\theta$ denotes the dot product between the ambient current velocity and the unit wavenumber vector along the wave propagation direction. Eq. (4) represents a newly defined wavenumber considering the diffraction due to the presence of structures, rapid change of bathymetry and current fields. The substitution of Eq. (5) into Eq. (4) results in the new wavenumber owing to the wave diffraction effect:

$$K = k\delta_n \tag{6}$$

where δ_n represents a refraction–diffraction correction parameter expressed as

$$\delta_n = \frac{1}{\left(\frac{U_s}{c}\right)^2 - n}\left\{\frac{U_s}{c}\left(1+\frac{U_s}{c}\right) - \sqrt{\left(\frac{U_s}{c}\right)^2\left(1+\frac{U_s}{c}\right)^2 - n\left[\left(\frac{U_s}{c}\right)^2 - n\right]\delta_a}\right\} \tag{7}$$

where δ_a is a parameter including the effect of the current and is written in the form of

$$\begin{aligned}\delta_a = 1 &+ \frac{\nabla_h\cdot\left(cc_g\nabla_h a\right)}{k^2 cc_g a} + \frac{f_1 g\nabla_h^2 h + f_2 gk|\nabla_h h|^2}{k^2 cc_g} \\ &+ \frac{1}{n}\left(2+\frac{U_s}{c}\right)\frac{U_s}{c} - \frac{\nabla_h\cdot[\boldsymbol{U}(\boldsymbol{U}\cdot\nabla_h a)]}{k^2 cc_g a}\end{aligned} \tag{8}$$

and

$$n = \frac{1}{2}\left(1+\frac{2kh}{\sinh 2kh}\right) \tag{9}$$

The EMSE used in the present model is only valid for propagating waves. Non-propagating (evanescent) modes are not considered in the mathematical formulation. Therefore, we note that K is not realistic if the square root is imaginary. In the limiting case of the absence of the ambient current and the elimination of a rapidly varying bottom seabed, Eq. (7) is readily reduced to the eikonal equation provided by Holthuijsen et al. (2003)

$$K = k\delta_m = k\sqrt{1+\frac{\nabla_h\cdot\left(CC_g\nabla_h a\right)}{k^2 cc_g a}} = k\sqrt{1+\frac{\nabla_h^2 a}{ka^2}+\frac{\nabla_h\left(CC_g\right)\cdot\nabla_h a}{k^2 CC_g a}} \tag{10}$$

where δ_m is the refraction–diffraction correction parameter obtained from the conventional MSE. It has been shown by Holthuijsen et al. (2003) that δ_m accounts for the diffraction-induced directional turning rate in the SWAN model (Booij et al., 1999).

According to Eq. (6), the diffraction-correction phase speed C can be obtained as follows.

$$C = \frac{\omega}{K} = \frac{c+U_s}{\delta_n}. \tag{11}$$

Substituting the velocity potential into Eq. (1), the imaginary part leads to the energy transport equation after multiplying the wave amplitude a:

$$\nabla_h\cdot\left\{\left[CC_g\nabla_h S + (\omega - \boldsymbol{U}\cdot\nabla_h S)\boldsymbol{U}\right]a^2\right\} = 0. \tag{12}$$

Using the relations $\boldsymbol{K} = \nabla_h S$, $K = k\delta_n$ and $c = \sigma/k$, Eq. (12) is in terms of the energy transport equation given by

$$\nabla_h\cdot\left\{\left[\delta_n c_g + \left(1+\left(\frac{U_s}{c}\right)(1-\delta_n)\right)\boldsymbol{U}\right]a^2\right\} = 0 \tag{13a}$$

$$\text{or}\quad \nabla_h\cdot\left(\boldsymbol{C}_g E\right) = 0. \tag{13b}$$

Based on Eq. (13), it is seen that a modified wave propagation velocity with the current effect (Eq. (13a)) is represented by the conventional wave energy conservation equation (Eq. (13a)). Therefore, the energy propagation speed due to the diffraction and current effects in the geographic space is written as

$$C_g = \delta_n c_g + \left[1+\left(\frac{U_s}{c}\right)(1-\delta_n)\right]\boldsymbol{U} \tag{14}$$

where $\boldsymbol{C}_g = (C_x, C_y)$, C_x and C_y are the wave energy propagation velocities due to the diffraction with current and higher-order bottom effects in the x- and y-components, respectively. In the absence of currents and higher-order bottom effects, Eq. (14) is reduced to $\boldsymbol{C}_g = \delta_m c_g$ which is identical to the theory of Holthuijsen et al. (2003).

If the source term representing the processes of wave generation, dissipation and nonlinear wave–wave interactions is retained, then the energy equation is written in the form (Janssen et al., 1994)

$$\nabla_h\cdot\left(C_g E\right) = \tilde{S} \tag{15}$$

where $\tilde{S}$ is the source term of wave energy to account for wave generation, dissipation and nonlinear wave–wave interactions. By comparing Eqs. (14) and (15), we note that the phase-decoupled model includes wave–wave interaction when it is based on a local linear approach.

3. Modified wave action balance equation

The evolution of the wave spectrum is described by the wave action balance equation (e.g., Hasselmann et al., 1973), which is used in the wind wave model of the SWAN. The equation is expressed by Cartesian coordinates:

$$\frac{\partial N}{\partial t} + \frac{\partial}{\partial x}(c_x N) + \frac{\partial}{\partial y}\left(c_y N\right) + \frac{\partial}{\partial\sigma}(c_\sigma N) + \frac{\partial}{\partial\theta}(c_\theta N) = S_{total} \tag{16}$$

where $N = N(\sigma,\theta)$ is the wave action density spectrum; t the time; c_x and c_y the wave propagation velocities in x and y components, respectively; c_σ and c_θ the wave propagation velocities in σ and θ coordinates, respectively; $S_{total} = \tilde{S}/\sigma$ the source term in terms of energy density representing the processes of wave generation, dissipation and nonlinear wave–wave interactions.

Adding wave diffraction to the action balance equation involves only replacing c_x, c_y, c_σ and c_θ by the correction corresponding propagation speeds C_x, C_y, C_σ and C_θ with the aid of δ_n. When the wave diffraction is included and the phase-decoupled approximation is used, the expressions for the wave propagation speeds are modified by the change of the directional turning rate of a single wave component as it travels along the wave ray with the group velocity. Using Eq. (14), the resulting expressions for the propagation speeds in the geographic and spectral spaces are given, respectively, by

$$C_x = \delta_n c_g\cos\theta + \left[1+\left(\frac{U_s}{c}\right)(1-\delta_n)\right]U_x \tag{17}$$

$$C_y = \delta_n c_g\sin\theta + \left[1+\left(\frac{U_s}{c}\right)(1-\delta_n)\right]U_y \tag{18}$$

$$C_\sigma = \frac{\partial\sigma}{\partial h}\left[\frac{\partial h}{\partial t} + U_x\frac{\partial h}{\partial x} + U_y\frac{\partial h}{\partial y}\right] - \delta_n c_g k\left(\cos\theta\frac{\partial U_s}{\partial x} + \sin\theta\frac{\partial U_s}{\partial y}\right) \tag{19}$$

$$\begin{aligned}C_\theta = c_g\delta_n&\left[\frac{1}{k}\left(\sin\theta\frac{\partial k}{\partial x} - \cos\theta\frac{\partial k}{\partial y}\right) + \frac{1}{\delta_n}\left(\sin\theta\frac{\partial\delta_n}{\partial x} - \cos\theta\frac{\partial\delta_n}{\partial y}\right)\right] \\ &+ \left(\sin\theta\frac{\partial U_s}{\partial x} - \cos\theta\frac{\partial U_s}{\partial y}\right).\end{aligned} \tag{20}$$

Referring to Eqs. (7) and (8), we notice that δ_n includes the combined effects of a, $|\nabla_h h|$, and $\nabla_h^2 h$ and U_s. Holthuijsen et al. (2003) indicated that the diffraction of random, short-crested waves can also be computed as the superposition of solutions for a number of incident monochromatic, directional waves. Each component is calculated independently by the wave refraction and diffraction, but this method is impractical in the wave spectral model because of the problems of physical property such as ignorance of the wave–wave interaction as well as numerical convergence. For computational convenience in the phase-decoupled model, it is plausible to express the wave amplitude a in Eq. (7) by the square root of the summation of the wave action densities, that is

$$a = \sqrt{E} = \sqrt{\sum_{i=1}^{I}\sum_{j=1}^{J} \sigma_i N\left(\sigma_i, \theta_j\right) d\theta d\sigma} \tag{21}$$

where I and J are the total numbers of components in the wave frequency and direction spaces, respectively.

The inclusion of δ_n in the expressions of Eqs. (17)–(20) for the directional turning rate of the wave propagation velocities provides a straightforward way for the refraction–diffraction effect of the action balance equation to describe the wave transformation in the nearshore region. The present mathematical formulation indicates that the phase-decoupled approximation can account for the wave refraction, diffraction and reflection of the random waves for an arbitrary bathymetry in the presence of an ambient current.

By adding the refraction–diffraction correction parameter δ_n to the action balance equation, the expressions for the group velocity and the propagation velocities in the geographic and spectral spaces have been implemented in the WWM (Hsu et al., 2005). A numerical model was developed in the WWM using FEM for wind wave simulations in both large-scale oceanic deep water and small-scale shallow water regions. The FEM code with unstructured grids improves the numerical scheme of the nested grids to maintain the computational efficiency and accuracy for practical applications.

The wave reflection from natural beaches and man-made coastal and marine structures influences the hydrodynamics, the currents and the sediment transport in the front of the reflector. It is of great importance to estimate the nature of the reflection coefficients accurately in many coastal applications. The wave refraction, diffraction and reflection effect are the focus of the present study. Referring to Ardhuin and Herbers (2002), wave reflection is also involved in the refraction–diffraction approximation in the WWM.

Notably the propagation speed of the directional space in Eq. (16) includes fourth-order derivatives of the wave amplitude a. The resulting calculation is unstable and oscillates because of the higher-order derivatives. Holthuijsen et al. (2003) used a convolution filter in the geographical space to decrease these instabilities. Later, a numerical sound solution to the instability problem is under-relaxation as used by Holthuijsen (2007). However, the traditional convolution filter is not easy to apply in the WWM due to the unstructured grid system, the value of a is thus smoothened by the following averaged spatial filter,

$$a_i^{n+1} = \frac{1}{Q}\sum_{j=1}^{Q} a_j^n \tag{22}$$

where the superscript n denotes the number of iterations for the smoothing procedure and Q represents the number of nodes connecting to the i-th node of the unstructured mesh. This filter was used as the averaged spatial filtering applied to each individual node. The divergence of the wave energy $\nabla_h \cdot \left(cc_g \nabla_h \sqrt{\sigma N}\right)$ in the expression of δ_n is thus obtained using the smoothing filter.

In each time step of the computation δ_n is calculated by Eqs. (7) and (8). The new smoothened wave amplitude a is obtained for each grid point and is only used to estimate the value of δ_n with the help of Eq. (7) and replace k by the wavenumber K, while the directional turning rate of the wave propagation speeds C_x, C_y, C_σ and C_θ are corrected using Eqs. (17)–(20). The value of a is only smoothened and is not iterated in the convolution filter, therefore there is no need to define the maximum tolerance level in the model. The number of iterations for smoothing is controlled by the parameter $L/2\Delta x$, where L is the local wavelength and Δx is the grid size. The parameter $L/2\Delta x$ means that the number of the grid points $L/\Delta x$ is prescribed in a wavelength for accurately describing the wave profile and the denominator is used as a relaxation coefficient for numerical stability. It is expected that the number of iterations for smoothing should result in a higher resolution of the wind wave simulation.

All the new correction propagation velocities are inserted into the action balance equation to solve the spectral density N. The estimation of δ_n is repeated based on the values of the action density N obtained from the preceding iteration.

4. Relative importance of additional terms

In this section the relative importance of the additional terms of δ_n is examined in order to know the contribution of these influencing factors, which include the wave amplitude $\nabla_h a/ka$, bottom slope $\nabla_h h/kh$, bottom curvatures $\nabla_h^2 a/k^2 a$, and $\nabla_h^2 h/k^2 h$ and the ambient current strength U_s/c. It should be noted that the difference between the present theory and the approximation of Holthuijsen et al. (2003) is reflected in the different eikonal equation as given in Eq. (7). For convenience, the second term on the right-hand side of Eq. (8) is further rearranged using the spatial differentiation $\nabla_h(cc_g) = (\partial cc_g/\partial h)\nabla_h h + (\partial cc_g/\partial k)\nabla_h k$. To have a simple expression of δ_n in the analysis, a one-dimensional uniform current $U_s = U$ is also assumed. These expressions are then substituted into Eq. (8) to yield the following expression:

$$\begin{aligned}\delta_a = 1 &+ f_1 \frac{kh}{n\ tanh\, kh}\frac{\nabla_h^2 h}{k^2 h} + f_2 \frac{(kh)^2}{n\ tanh\, kh}\left|\frac{\nabla_h h}{kh}\right|^2 + f_3 \frac{\nabla_h h}{kh}\cdot\frac{\nabla_h a}{ka} \\ &+ \frac{2}{n}\frac{U}{c} + \frac{1}{n}\left(\frac{U}{c}\right)^2 - \frac{1}{n}\left(\frac{U}{c}\right)^2 \frac{\nabla_h^2 a}{k^2 a} + \frac{\nabla_h^2 a}{k^2 a}\end{aligned} \tag{23}$$

in which f_3 is given by

$$f_3 = \frac{kh\left(1 - tanh^2 kh\right)(3\ tanh\, kh + kh - 3kh\ tanh\, kh)}{tanh^2 kh + kh(1 - tanh^2 kh)(2\ tanhkh + kh - kh\ tanh^2\, kh)}. \tag{24}$$

For the simple case of the refraction approximation to be a valid one, then $\delta_n = 1$ and $K = k$, and Eq. (7) shows that the following conditions should be met:

$$\frac{\nabla_h h}{kh} \approx \frac{\nabla_h^2 h}{k^2 h} << 1,\ \frac{\nabla_h a}{ka} \approx \frac{\nabla_h^2 a}{k^2 a} << 1, \text{ and } \frac{U_s}{c} << 1. \tag{25}$$

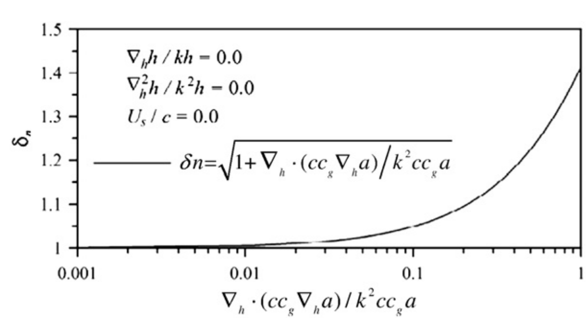

Fig. 1. Relationship of δ_n versus $\nabla_h \cdot (cc_g \nabla_h a)/k^2 cc_g a$ without current effect.

For the combined wave refraction–diffraction on a horizontal bottom without current, i.e. $|\nabla_h h| = \nabla_h^2 h = U_s/c = 0$, Eq. (7) is reduced to the following expression with the help of Eq. (25).

$$\delta_m = \sqrt{1 + \frac{\nabla_h^2 a}{k^2 a}}. \tag{26}$$

The term $\nabla_h^2 a/k^2 a$ accounts for the effect of the diffraction for travelling waves at a constant water depth. The importance of δ_n in terms of the eikonal equation (Eq. (10)) proposed by Holthuijsen et al. (2003) is shown in Fig. 1. It is evident that δ_n increases with the increase of $\nabla_h \cdot (cc_g \nabla_h a)/k^2 cc_g a$, indicating that a larger curvature of the wave amplitude $\nabla_h^2 a/k^2 a$ and the spatial rate of the directional turning due to the varying wave speed $(\nabla_h cc_g)$ would produce a larger wave diffraction. To have a better understanding of the factors influencing δ_n, a slow scale β is introduced to express the order of magnitude in each of the additional terms in Eq. (7), in which the water surface elevation is written as $\varsigma = a(\beta \boldsymbol{X})e^{iS}$ and $\boldsymbol{X} = (x, y)$ is the position vector. We then have $\nabla_h h/kh = \nabla_h a/ka = O(\beta)$ and $\nabla_h^2 h/k^2 h = \nabla_h^2 a/k^2 a = O(\beta^2)$ for the condition of the refraction effect only being valid. The order of $\beta = 0.01$ is chosen as an index of the influencing factors in the present study.

Fig. 2(a) illustrates that δ_n is a function of the relative water depth kh for different values of $\nabla_h h/kh = \beta^0, \beta^{1/2}$ and β while $\nabla_h a/ka = \nabla_h^2 a/k^2 a = 1.0$. The results show that δ_n increases with the decreasing relative water depth. Note that a larger value of δ_n could be obtained at a shallow water depth. Meanwhile, a steeper bottom slope would lead to a larger value of δ_n, when the order of the slope and the curvature of the wave amplitude are supposed to be at the higher

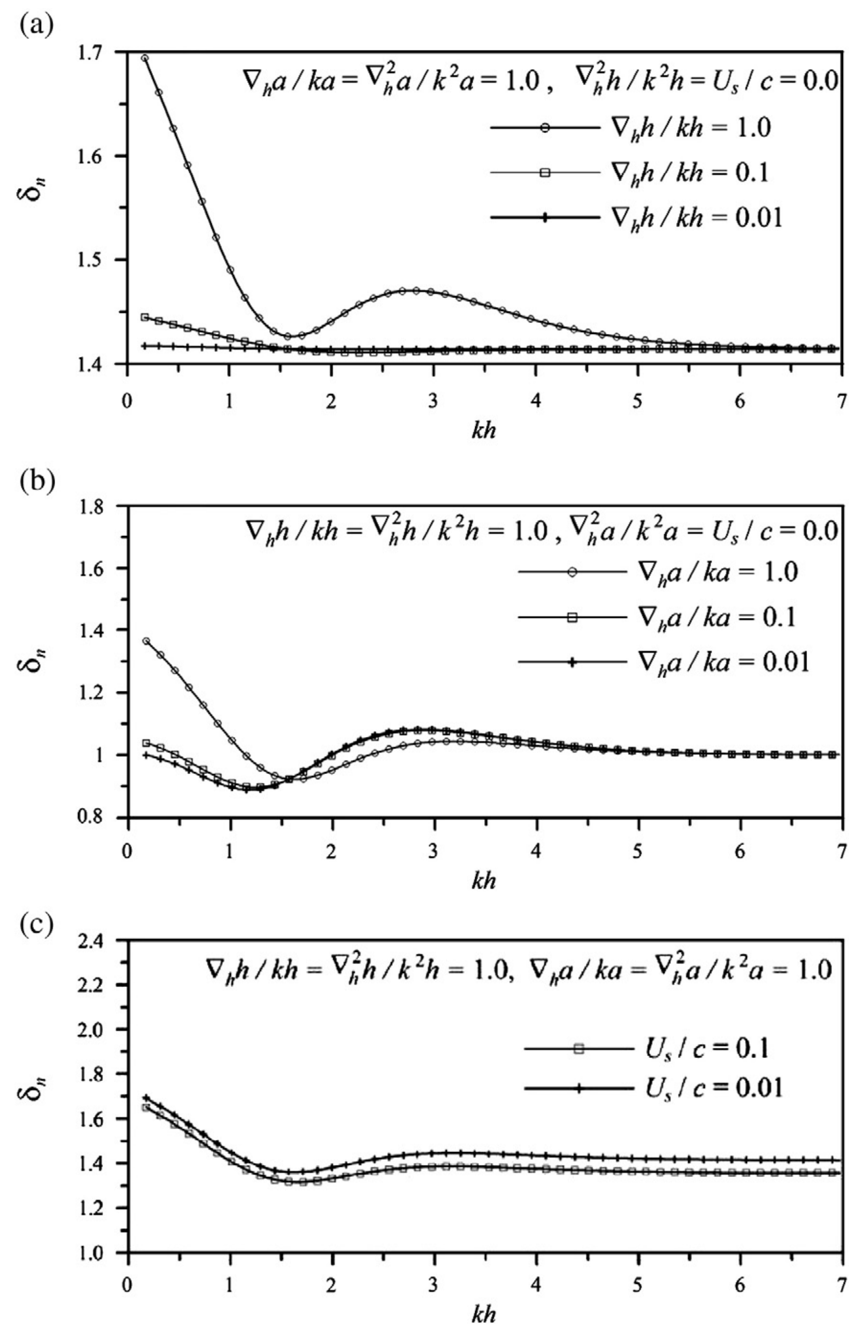

Fig. 2. (a) Relationship of δ_n versus kh for various bottom slopes $\nabla_h h/kh$, (b) relationship of δ_n versus kh for various wave amplitude slopes $\nabla_h a/ka$, and (c) relationship of δ_n versus kh for various current velocities U_s/c.

value of $\nabla_h a/ka = \nabla_h^2 a/ka^2 = 1$. We thus conclude that the effect of rapidly varying bathymetry on the wave diffraction becomes important in the shallow water region for the case of $\nabla_h a/ka = \nabla_h^2 a/ka^2 = 1$ without the current effect. Fig. 2(b) displays δ_n as a function of kh for three different values of the wave amplitude slope $\nabla_h a/ka = 1$, 0.1 and 0.01 for the cases of the bottom slope and curvature $\nabla_h h/kh$ and $\nabla_h^2 h/k^2 h$ of $O(1)$. It is found that the effect of the wave amplitude slope on δ_n becomes notable with the increase of $\nabla_h a/ka$ in the shallow water region. The value of δ_n increases with the decrease of the relative water depth kh. A larger value of the wave amplitude slope would yield a larger value of δ_n for a rapidly varying bottom configuration. The combined effect of the wave profile, bathymetry and current on the diffraction-correction parameter is presented in Fig. 2(c). In the figure, two typical current strengths $U_s/c = 0.1$ and 0.01 are considered for $\nabla_h h/kh = \nabla_h a/ka = 1$. It is evident that a larger relative current velocity would produce a smaller value of δ_n when the relative water depth decreases.

To illustrate how realistic the ranges of parameters shown in Figs. 1 and 2, we take a practical example of the significant wave height of $H_{1/3} = 1\ m$ (wave amplitude $a = 0.5\ m$), wave period of $T_{1/3} = 5$ s, water depth of $h = 10\ m$ to calculate the values of the bottom slope, the curvature of the wave profile and the current velocity. The results are $\nabla_h h = 1.717$; 0.1717 and 0.01717 for $\nabla_h h/kh = 1.0$; 0.1 and 0.01; $\nabla_h^2 a = 1.47 \times 10^{-4}\ m^{-1}$; $1.47 \times 10^{-3}\ m^{-1}$; $1.47 \times 10^{-2}\ m^{-1}$ for $\nabla_h^2 a/k^2 a = 0.01$; 0.1 *and* 1.0; $U_s = 0.73186$ m/s and 0.073186 m/s for $U_s/c = 0.1$ *and* 0.01. Clearly, the calculated physical quantities match very well in the nature of the practical conditions.

5. Model validation

Notably the present model is based on a phase-averaged approximation; the wave phase cannot be resolved in the numerical simulation. The main purpose of adding the phase-decoupled refraction–diffraction approximation to the action density equation for a rapidly varying sea bottom with the current effect is to obtain a reasonable estimate of the wave diffraction in a computation of the WWM. Verifying the validity of the present model requires observations or superior computations with convincing diffraction effects. Unfortunately, they are unavailable due to the difficulty of obtaining measurements in the real situations. Instead, as done by previous researchers, we consider small-scale computations for which measurements are available from the laboratory tests. Different numerical cases were also tested under such conditions of random, short-crested wave transformations over a rapidly varying bottom with significant diffraction effects in the presence of currents. In this study, four cases were carried out to validate the refraction, diffraction and reflection correction parameter with higher-order terms. If the model performs reasonably well in these conditions, it will almost certainly function well within the proper range of applications.

As for the inclusion of the wave reflection in the WWM, we follow the method proposed by Ardhuin and Herbers (2002). The triad wave–wave-bottom interaction source term S for the spectral energy balance equation yields to the reflection estimates for a localized scatter. The bottom elevation is represented by small bottom amplitudes δ^* and the mean water depth h. The wave–bottom interaction source term is given by (Ardhuin and Herbers, 2002)

$$S(\boldsymbol{k}) = 4\pi g^{1/2} h^{-9/2} \chi(kh) \int_0^{2\pi} \cos^2(\theta - \theta') F^B(\boldsymbol{k} - \boldsymbol{k}') [E(\boldsymbol{k}') - E(\boldsymbol{k})] d\theta' \tag{27}$$

$$\text{with } \chi(kh) = \frac{(kh)^{9/2} \tanh kh^{1/2}}{\sinh 2kh(2kh + \sinh 2kh)} \tag{28}$$

where $\boldsymbol{k}$ is the wavenumber vector defined by $\boldsymbol{k} = (k \cos\theta, k \sin\theta)$, θ defines the travelling wave angle, $E(\boldsymbol{k})$ is the surface elevation spectrum and $F^B(\boldsymbol{k})$ is the small-scale bottom elevation spectrum obtained by discrete Fourier transform of the bottom. Details are referred to Ardhuin and Herbers (2002).

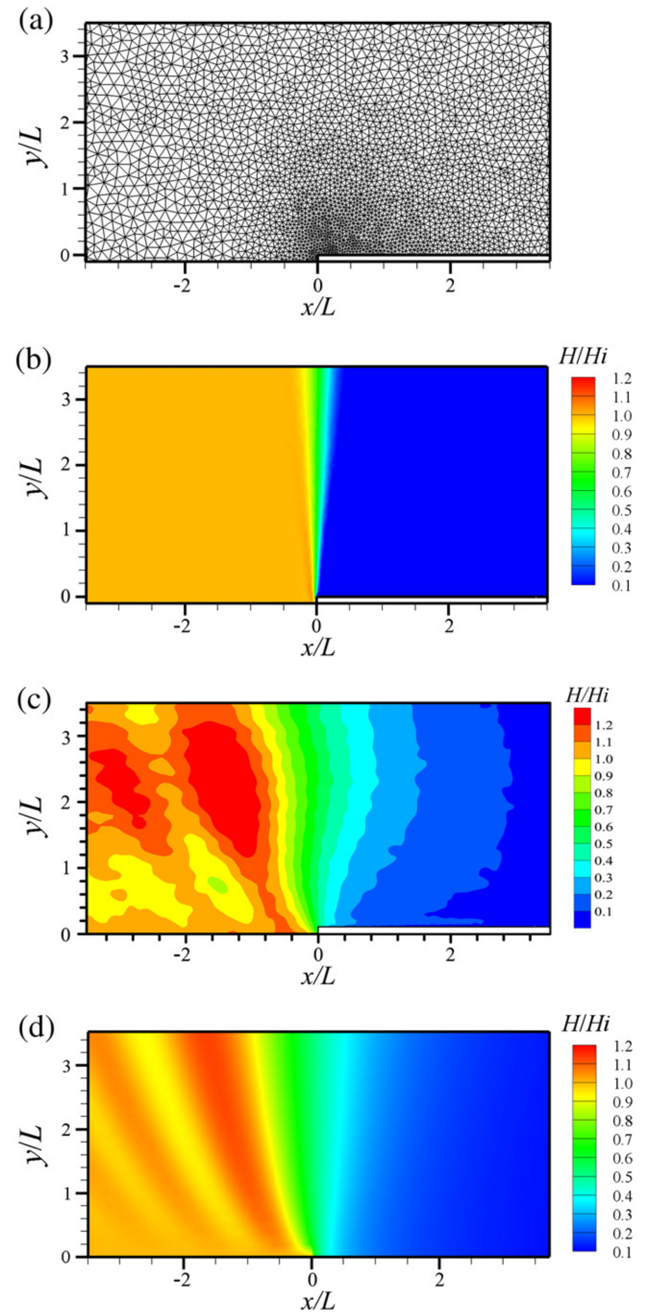

Fig. 3. Normalized wave height distribution around a semi-infinite breakwater. (a) Computational grids, (b) WWM without diffraction, (c) WWM with diffraction and (d) Sommerfeld solution.

5.1. Semi-infinite breakwater

Considering a vertical, rigid and semi-breakwater in the constant water depth, the effect of diffraction on the directional turning rate of the waves is estimated by the present phase-decoupled approximation model. The unidirectional, monochromatic waves are approximated by a δ-spectrum, which is defined as one frequency with very narrow Gaussian directional distribution around the mean direction, approaching the breakwater perpendicularly from the bottom to the top as shown in Fig. 3. The incident wave height and period are 0.055 m and 1.30 s, respectively. In the computation, the directional spreading is taken as $\sigma_\theta = 1.5^0$ and the

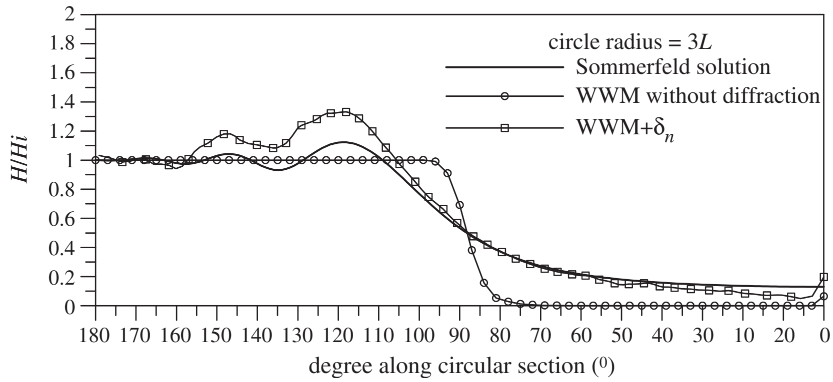

Fig. 4. Comparisons among numerical results of WWM without and with diffraction and the analytical solution of Sommerfeld along the circular section of 3*L*.

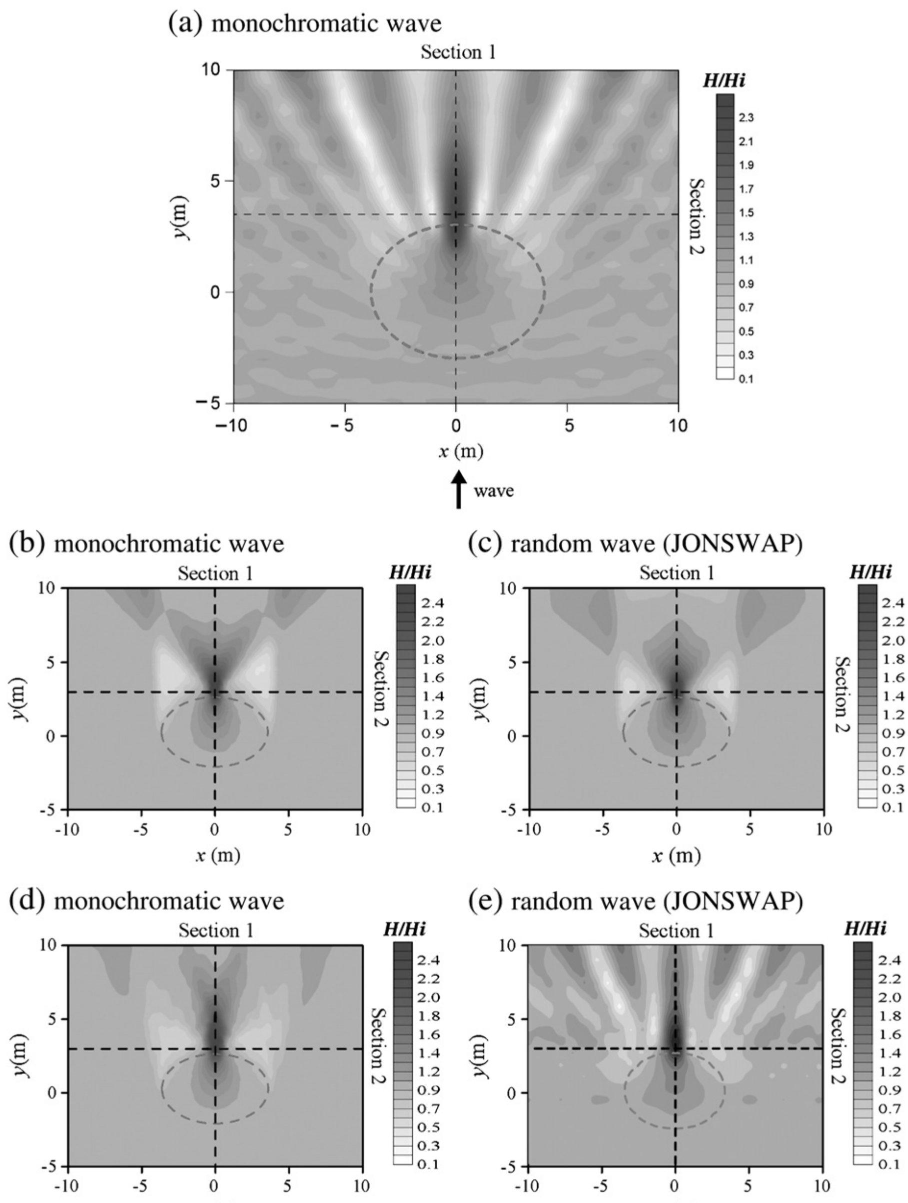

Fig. 5. Normalized wave heights for unidirectional waves propagating over an elliptical shoal. Section 1 is along the centre line of the domain and Section 2 is a line normal to the centre line behind the location of the elliptical shoal. (a) EEMSE (Hsu and Wen, 2001a); (b) and (c) WWM without diffraction; (d) and (e) WWM with diffraction.

directional resolution is chosen as $\Delta\theta = 0.25^0$. The wave field in this case can be obtained using the analytical solution of Sommerfeld in terms of the normalized wave height. It is clear from Fig. 3 that the pattern of wave heights predicted by the present phase-decoupled WWM model with diffraction (Fig. 3c) is in good agreement with the Sommerfeld's solution (Fig. 3d), but the results of the WWM without diffraction do not properly reproduce the wave pattern. Fig. 4 shows the comparison of the wave height at the circular section of 3L, where L is the wavelength. The wave height rising on the open side of the shadow line and in the area behind the breakwater is well reproduced by the WWM with δ_n. The present phase-decoupled model could not reproduce the oscillation of the Sommerfeld solution due to the phase averaged treatment in the wave balance equation.

5.2. Elliptical shoal

The present phase-decoupled model is applied to predict wave transformations over an elliptical shoal. The shoal rests at the bottom of a laboratory wave tank, and has major and minor radii of 3.96 m and 3.05 m, respectively. The experiment was conducted by Vincent and Briggs (1989) for waves propagating across the shoal, with significant refraction, diffraction and reflection effects and wave amplitude variations including caustics. The simulated monochromatic, unidirectional waves are the same as the wave conditions in the above section. Goda's (1999) JONSWAP spectrum is given by

$$S(f) = \sigma_1 \left(\frac{H_{1/3}}{T_p^2}\right)^2 f^{-5}\, exp^{\left[-1.25\left(T_p f\right)^{-4}\right]} \gamma^{exp\left[-\left(T_p f-1\right)^2/2\sigma_0\right]} \tag{29}$$

where γ is the peak enhancement factor, $\sigma_1 = 0.2189$ the spectral parameter, $T_p = 1/f_p$ the peak period, $\sigma_0 = 0.07$as $f \le f_p$ and $\sigma_0 = 0.09$ as $f \ge f_p$.

For the case of the irregular waves, the incident wave with a narrow JONSWAP spectrum $\gamma = 22$ and a narrow Gaussian directional distribution were implemented in the laboratory experiments of Vincent and Briggs (1989). The incident significant wave height is $H_{1/3} = 0.0254$ m

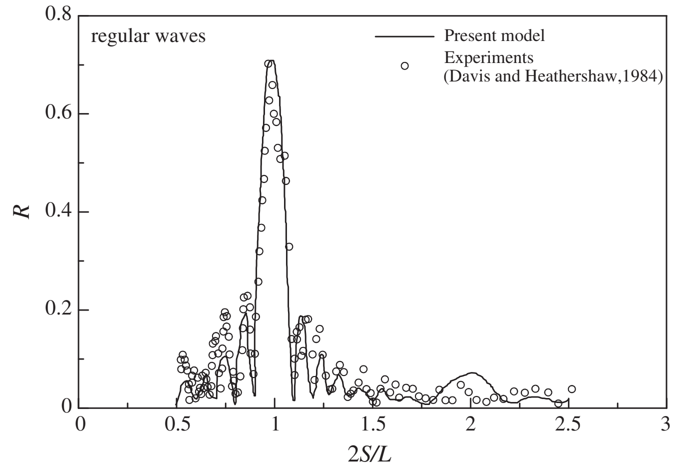

Fig. 7. Comparisons between laboratory experiments of Davies and Heathershwa (1984) and numerical simulations of Bragg scattering by WWM for regular waves.

and the peak period is $T_p = 1.3$ s, respectively. The incident directional spreading is $\sigma_\theta = 3°$ and the directional resolution is $\Delta\theta = 0.3°$.

The computational results are compared with the experiments of Vincent and Briggs (1989) and with the numerical results of the EEMSE (Evolution Equation of MSE) developed by Hsu and Wen (2001a). The normalized wave height for the monochromatic and random waves is presented in Fig. 5. The computational results of the WWM (Fig. 5(d) and (e)) shows that using the phase-decoupled refraction approximation without diffraction (Fig. 5(b) and (c)) will spread the effect of the shoal on the wave pattern over a larger area. Notably the wave field with the approximation δ_n in the case of the random waves (Fig. 5(e)) is almost the same with that of the monochromatic case (Fig. 5(d)). The wave convergence calculated by the EEMSE (Fig. 5(a)) and WWM with the diffraction of higher-order bottom slope terms and reflection (Fig. 5(e)) is more visible than that of the WWM with only the refraction (Fig. 5(d)). The comparison of

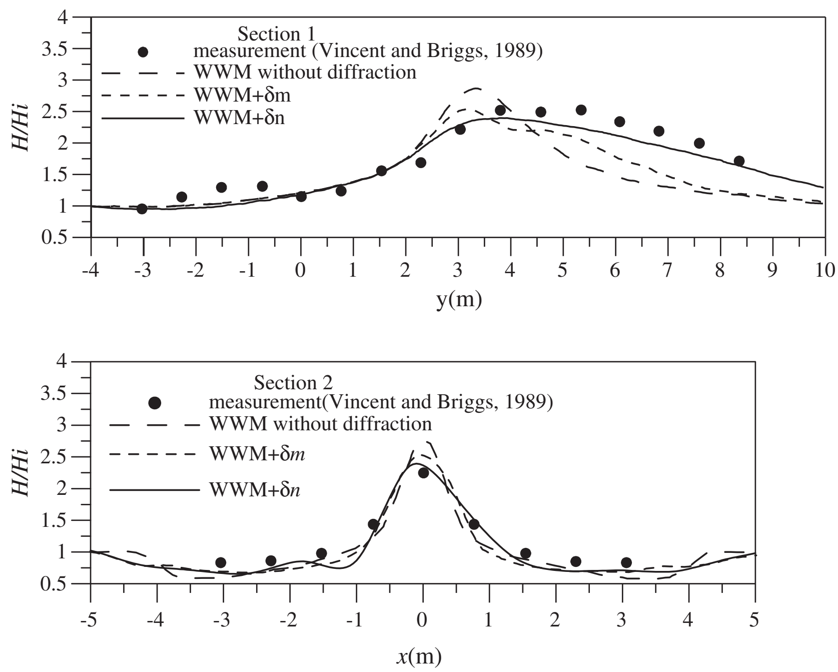

Fig. 6. Comparisons between observations of Vincent and Briggs (1989) and wave heights calculated by WWM with and without diffraction at Sections 1 and 2. δ_m: derived from MSE; and δ_n: derived from EMSE.

Fig. 5(b) and (d) implies that the WWM model with the present phase-decoupled approximation predicts a smoother wave height distribution than without the diffraction.

The computational results are also presented along with two lines: the centre line of the tank (Section 1) and the line normal to the centre line (Section 2) that is located just behind the shoal, as shown in Fig. 5. The comparisons at Sections 1 and 2 are shown in Fig. 6. Notably there are significant discrepancies between the results of δ_n and δ_m and the higher-order bottom effect of the phase-decoupled approximation yields a better estimation of the wave height around the shoal.

5.3. A series of submerged breakwaters

For water waves propagating over a patch of seabed, Bragg scattering occurs when the surface wavenumber is equal to one-half of the wavenumber of the undulating bottom. In this condition, the reflected waves will return in equal phases with the forward waves and enhance each other as they match the condition given above. Ardhuin and Herbers (2002) presented a phase-averaged model to account for the Bragg reflection for random waves travelling over an irregular seabed. Wave reflection is included in the present model. The scattering due to the wave refraction, diffraction and reflection is also important for waves passing over a series of submerged breakwaters in practical applications of coastal protection.

Several numerical simulations were performed to investigate the effect of higher-order bathymetric terms on the Bragg scattering, particularly for the case of the wave refraction, diffraction and reflection of over sinusoidal or artificial undulations (e.g. Chamberlain and Porter, 1995a; Chandrasekera and Cheung, 1997; Lee et al., 1998; Hsu and Wen, 2001a). Their computational results confirm that the inclusion of the bottom slope and second-order horizontal derivatives in the MSE is able to provide better reflection coefficients at the resonant peak.

Although the main purpose of this study focuses on the irregular waves, it is instructive to compare the results of the phase-decoupled model with Davies and Heathershwa's (1984) laboratory experiments. The δ-spectrum of Eq. (29) is again approximated to simulate the Bragg scattering of regular waves propagating over sinusoidal undulations. Fig. 7 shows the nature of the dependence of the reflection coefficient R on the dimensionless parameter $2S/L$ under the experimental conditions of $D=0.05$ m, $S=1.0$ m, $M=10$, $h=0.313$ m, $D/h=0.16$, where D and M are the amplitude and the number of bars, respectively, and S is the periodic bar spacing. We note that the numerical results are compared favorably with the experimental data.

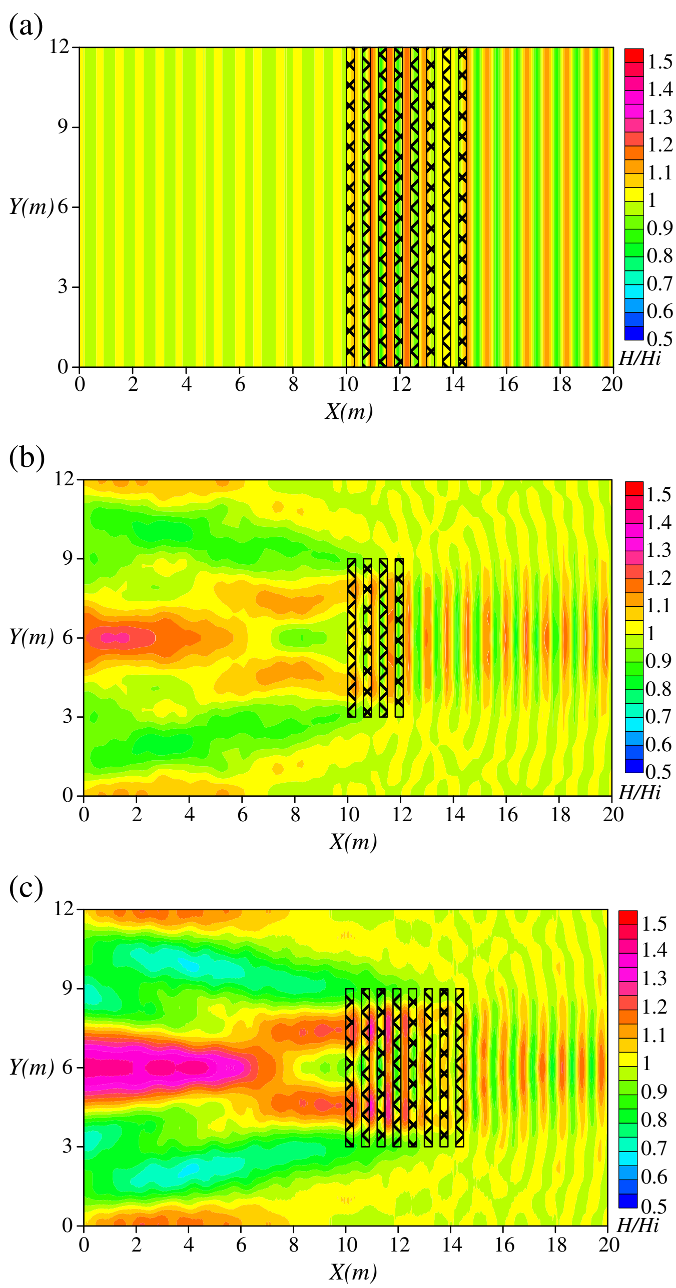

Fig. 8. Normalized wave height patterns for irregular waves travelling over a series parallel submerged breakwater; (a) 8 units of breakwater with infinite length; (b) 4 units of breakwater and (c) 8 units of breakwater with finite lengths. The results were calculated by the correction parameter δ_n and wave–bottom interaction source term $S(k)$.

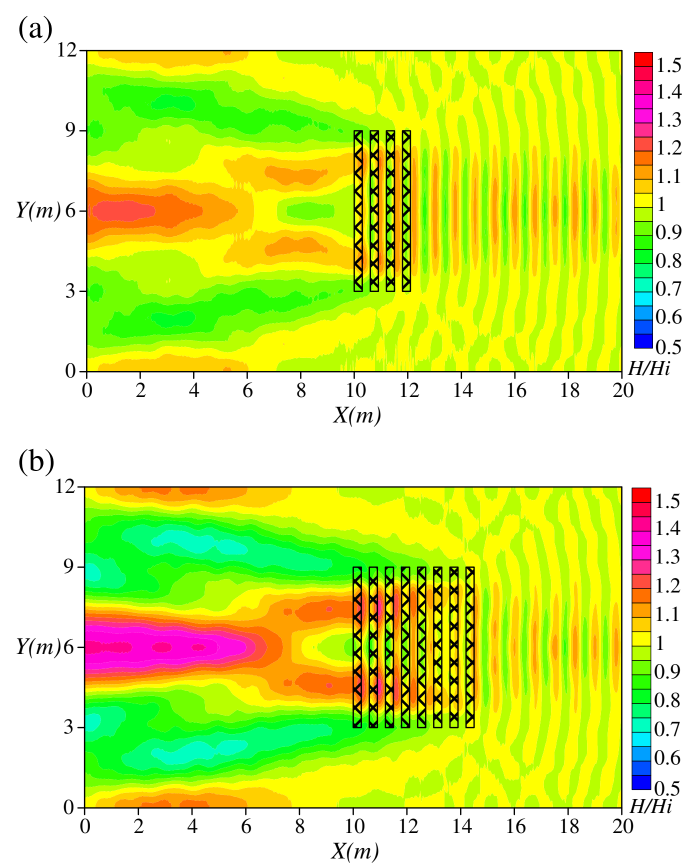

Fig. 9. Normalized wave height patterns for regular waves travelling over a series of parallel submerged breakwater; (a) 4 units of breakwater with finite length; and (b) 8 units of breakwater with finite length. The results were calculated by the correction parameter δ_n and wave–bottom interaction source term $S(k)$.

The present model computes the Bragg scattering of water waves propagating over a series of submerged parallel breakwaters. Fig. 8(a), (b) and (c) shows the computational results of the wave pattern for the δ-spectrum wave and the bottom configurations consist of 4 and 8 units of the submerged breakwaters, respectively. The height of the breakwaters is $h_b = 0.25$ m, and the mean water depth over the breakwater is 0.25 m. The breakwaters are 12 m long and 0.35 m wide with a spacing of 0.35 m for infinite length and 6 m long for finite length, respectively. The normal incident monochromatic wave period and wave height are $T_{1/3} = 1.0$ s and $H_{1/3} = 0.04$ m, respectively, to produce a significant reflection. For irregular waves, the JONSWAP spectrum for the peak enhancement factor $\gamma = 3.3$ is chosen as the input condition in the model. The directional spreading is $\sigma_\theta = 3°$ and the directional resolution is discretized as $\Delta\theta = 0.3°$.

In Fig. 8, comparisons are made between the results of three different cases taking the effect of the wave diffraction and the number of breakwaters into account. Note that waves are converged in Fig. 8(b) and (c) behind the finite submerged breakwaters because of the wave diffraction at the tip of the breakwaters. It is evident that the refraction–diffraction correction parameter δ_n and the wave–bottom interaction source term $S(k)$ result in the Bragg scattering in front of the breakwaters and the larger wave heights on the down-wave end of the breakwaters.

The Bragg scattering of random waves by 4 and 8 units of parallel submerged breakwaters with finite length is presented in Fig. 9. The results are in terms of the triad wave–wave-structure interactions due to the combined effect of the wave refraction, diffraction and reflection. It is noted that the wave pattern of Fig. 9(a) and (b) are quite similar to those of Fig. 8(b) and (c) except that the Bragg reflection tends to become small. This might be caused by the spectral energy spreading in the processes of the Bragg scattering.

To have a better evaluation of the diffraction and reflection effects on the Bragg scattering, the wave height distributions along $x = 0{\sim}20$ m and $y = 6$ m; $x = 11$ m and 4 m, $y = 6{\sim}12$ m are plotted in Figs. 10 and 11, respectively. It is seen that the difference of wave heights obtained from δ_m and δ_n becomes noticeable in the region of $x = 0$ m to 10 m. This result implies that the inclusion of the higher-order bottom effect terms in δ_n could produce a pronounced refraction–diffraction effect of the Bragg scattering.

5.4. Jet-like current

To validate the application of the phase-decoupled wave model, numerical calculations are performed to investigate the wave refraction–diffraction owing to the wave–current interactions, which was originally studied by Arthur (1950) and later by Liu (1983). As shown in Fig. 12a, a

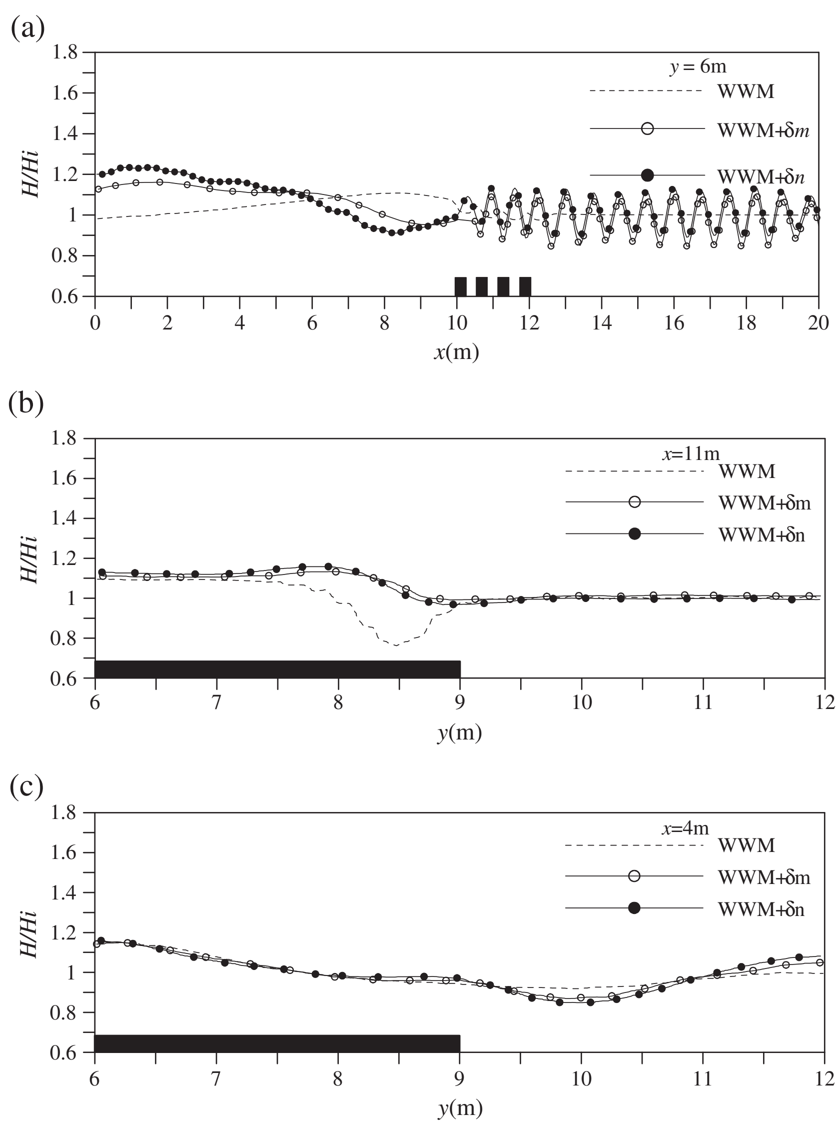

Fig. 10. Comparisons of the normalized wave height for waves propagating over a series of 4 submerged breakwaters along (a) $y = 6$ m, (b) $x = 11$ m and (c) $x = 4$ m.

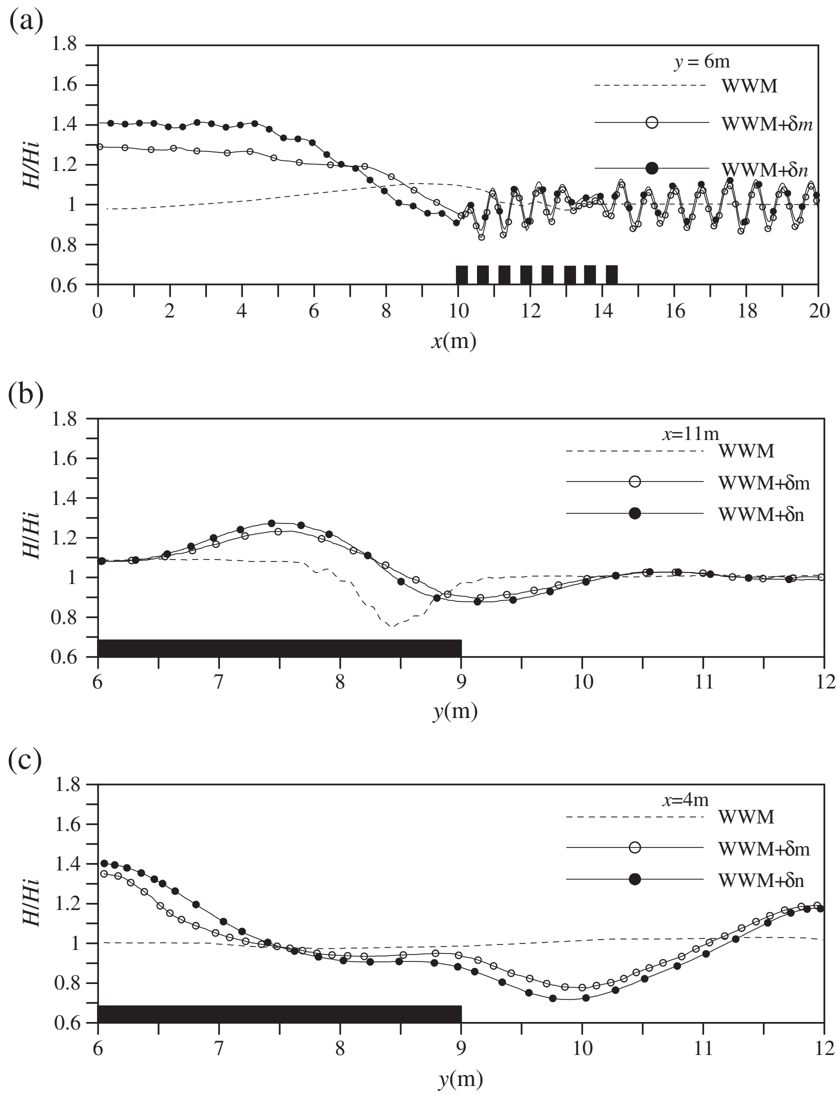

Fig. 11. Comparisons of the normalized wave height for waves propagating over a series of 8 submerged breakwaters along (a) $y=6$ m, (b) $x=11$ m and (c) $x=4$ m.

jet-like current system exists on a uniform sloping beach of 1/50. The current velocity is written as (Liu, 1983)

$$U_x = -1.73016\left[2-\left(\frac{y}{76.2}\right)^2\right]F\left(\frac{y}{76.2}\right)\int_0^{x/7.62}F(\alpha)d\alpha \tag{29}$$

$$U_y = 0.04395F\left(\frac{y}{76.2}\right)F\left(\frac{x}{7.62}\right) \tag{30}$$

with

$$F(\alpha) = \frac{1}{\sqrt{2\pi}}e^{-\alpha^2/2} \tag{31}$$

where the length and the time units are in meters and seconds, respectively. The normal incident monochromatic wave of $H_0=1$ m and $T=8$ s is generated at the boundary of $y=240$ m from the shoreline. Fig. 12 (b), (c) and (d) shows the computational meshes of the WWM model, a typical current velocity profile at the centerline and the distribution of the current field, respectively. The δ-spectrum is further used as the input condition in which the directional spreading is $\sigma_\theta=3°$ and the directional resolution is described as $\Delta\theta=0.3°$.

The contours of the dimensionless wave height due to the current effect obtained by Liu's (1983) parabolic approximation of the MSE are shown in Fig. 13(a). The wave height distribution obtained by the WWM without the diffraction correction is plotted in Fig. 13(b). The wave patterns of the WWM with δ_m and δ_n are presented in Fig. 13(c) and (d), respectively. All figures show that the offshore current, refraction and wave shoaling appear to enhance the growth of the wave height. Because the direction of an offshore current velocity component is opposite to that of the wave propagation, the effect of the offshore current would increase the local wave height. In Fig. 13(a), we notice that the longshore current component near the shoreline seems to produce a smaller local wave height in the range of $x=10$–30 m. Comparing Fig. 13(b) and (c), it is clear that the wave refraction–diffraction correction parameter could reduce the wave height in the opposite current region. A comparison of Fig. 13(a) and (d) indicates that the wave pattern in the region of $x=10$–30 m and $y=30$–90 m where the currents turn from the longshore direction to the offshore direction is quite similar to Liu's approximation. This result demonstrates that the WWM model incorporating the δ_n parameter is more capable of describing the wave refraction–diffraction for waves travelling on a sloping beach in the presence of a current. Notably the white-capping that dominates the wave field in a rip–current system does not exist in this case because no wind is the input and the wave

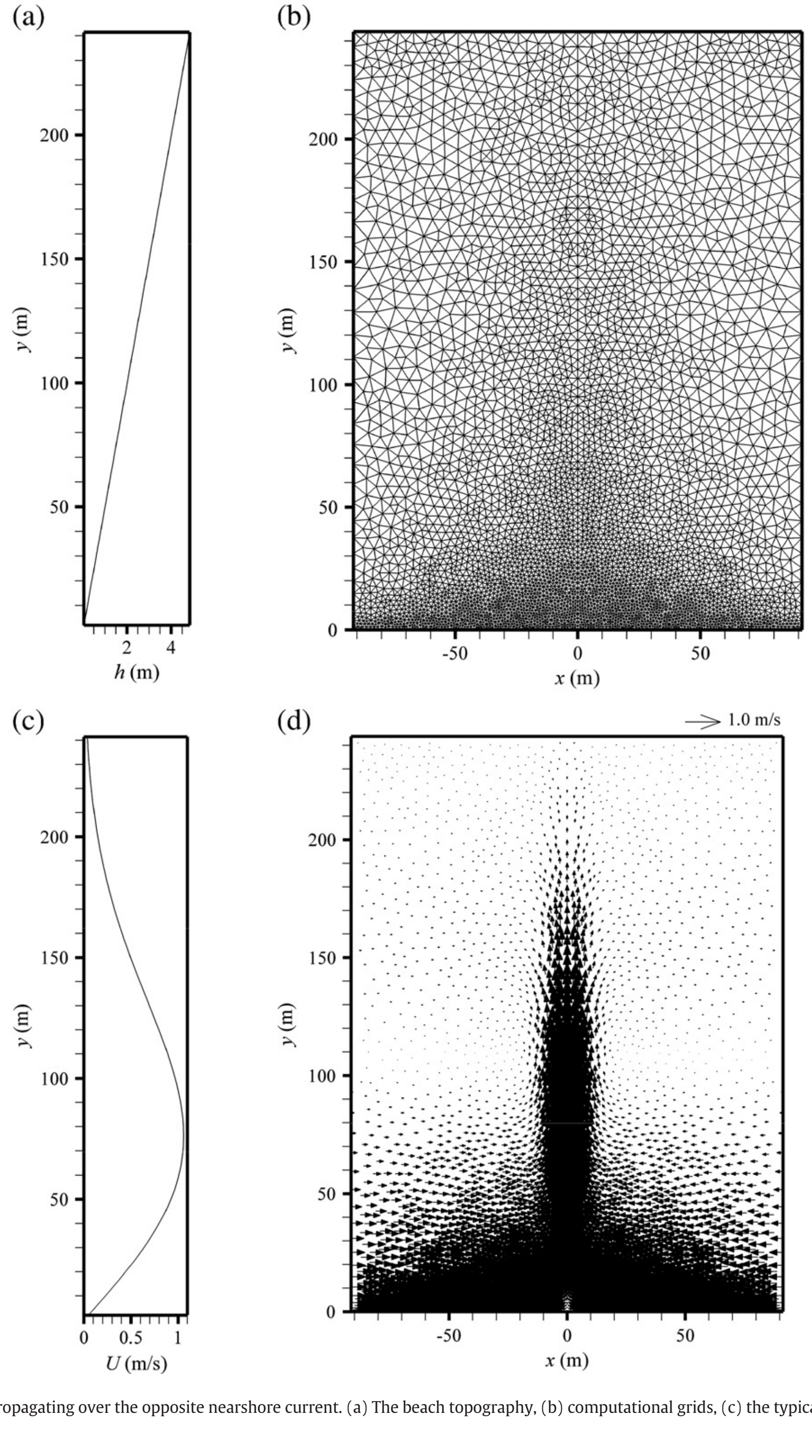

Fig. 12. Normal incident waves propagating over the opposite nearshore current. (a) The beach topography, (b) computational grids, (c) the typical current profile at centerline and (d) the nearshore current field.

condition is the δ-spectrum. Wave blocking may occur in this case resulting from the nearshore current in the opposite region.

To examine the current effect on the wave refraction–diffraction correction parameter, the dimensionless wave heights along the centre line ($x=0$) are plotted in Fig. 14(a). A relative error defined by $Er=|H-H_{\mathrm{MSE}}|/H_{\mathrm{MSE}}$ is used to evaluate the importance of the current effect on the refraction–diffraction correction parameter. The results of Er with and without the current-correction term are given in Fig. 14(b). From Fig. 14(a) it is interesting to note that the wave height increases monotonically only due to the shoaling and refraction effect without currents. The differences between the results of the Liu (1983) approximation and the WWM (with and without current effects) start to appear from $y=200$ m and increase rapidly shoreward. In Fig. 14(a), it is also clear that the effect of the jet-like currents reduce the wave height in the nearshore region. From Fig. 14(b), it is found that the WWM model with δ_n may decrease around a 10%

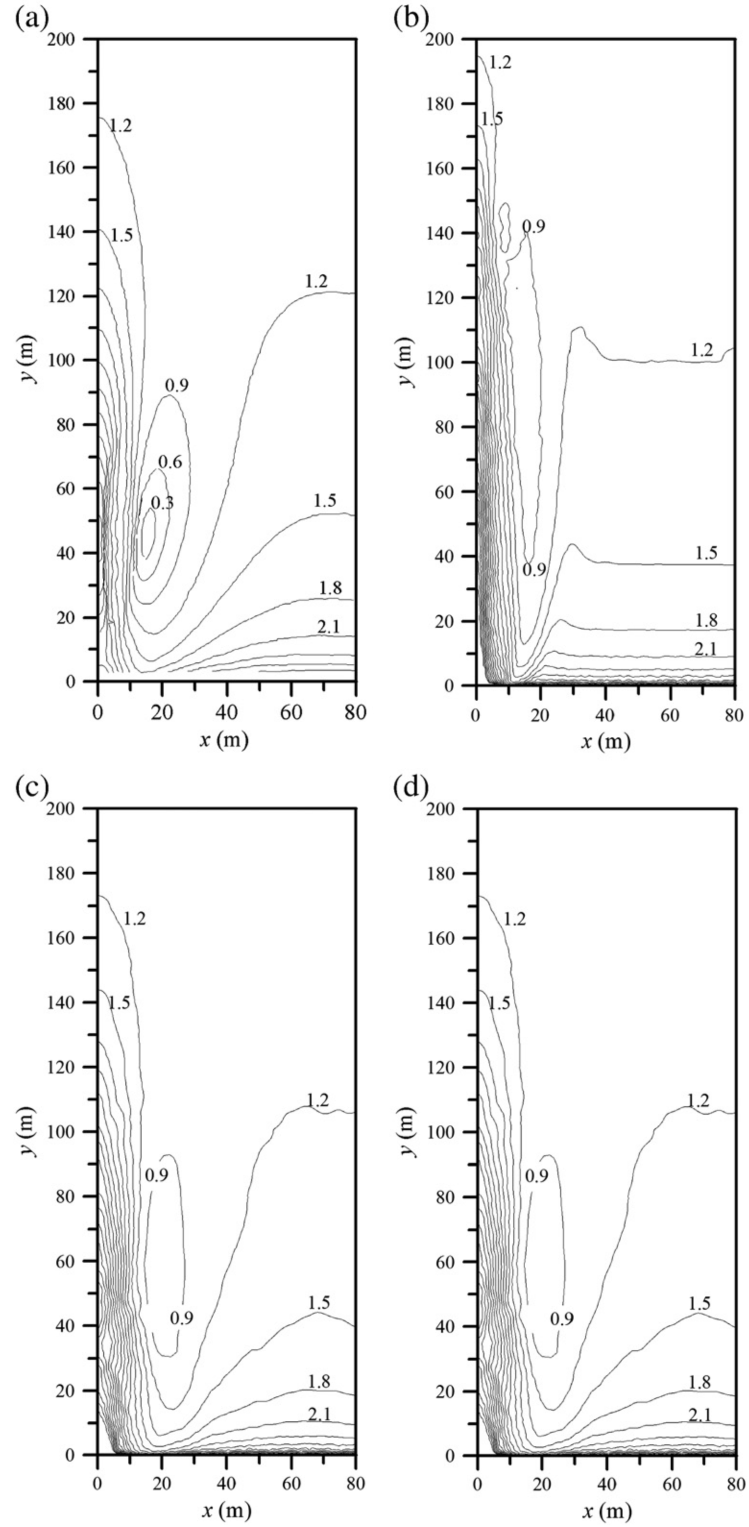

Fig. 13. The contours of normalized wave amplitude. (a) Liu (1983), (b) WWM without diffraction, (c) WWM with δ_m and (d) WWM with δ_n.

error when compared with Liu's approximation. The current speed relative to the wave phase speed U_s/c is presented in Fig. 14(c). This computational case is a typical example representing a realistic rip–current situation. In real situations, wave breaking often occurs and the nearshore currents can be driven by breaking waves toward the surf zone. However, this phenomenon is not considered in the present model.

6. Conclusions

Based on the EMSE, the phase-decoupled refraction–diffraction approximation for the waves propagating over a rapidly varying topography with an ambient current for the spectral wave model was developed in this study. The diffraction is assumed to be an additional parameter to the refraction/diffraction-induced directional turning

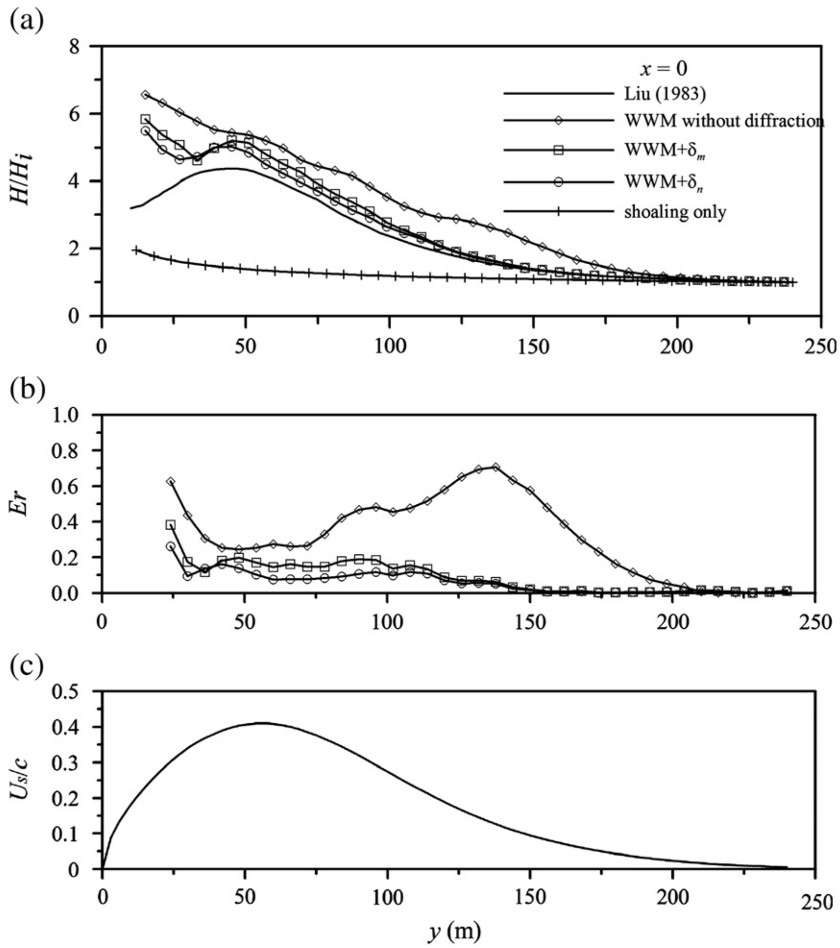

Fig. 14. Comparisons along the centerline of the currents ($x=0$). (a) Wave amplitude distributions, (b) relative errors ($Er=|H-H_{\mathrm{MSE}}|/H_{\mathrm{MSE}}$) and (c) the profile of U_s/c.

rate of the wave components in a given wave spectrum. The relative importance of the additional higher-order terms that influence the refraction–diffraction correction parameter is discussed. The model has been verified by five cases, and the computational results are in reasonably good agreement with observations or the results of the refraction, diffraction and reflection models.

The higher-order bottom slope and second-order horizontal derivative terms with the current effect derived from the EMSE provide more reasonable predictions where wave refraction and diffraction occur in the presence of a current on a rapidly varying sloping bottom. However, only the Liu's (1983) case considering currents, in which the wave propagating on a mild-slope was demonstrated in the present investigation. As aforementioned, several computational results by the EMSE or EEMSE indicated that a rapidly varying sea bottom could produce a larger wave reflection. Following Ardhuin and Herbers (2002), the problem of the Bragg scattering of water waves considering the effect of a rapidly varying topography solved by the phase-averaged model was also investigated. Wave reflection is included in the present model in which the scattering source term was implemented to solve the wave–wave-structure interaction problem. In summary, the proposed phase-decoupled wave model with the refraction–diffraction correction parameter can be applied to simulate wave scattering over an abruptly varying topography in the presence of an ambient current.

As discussed by Holthuijsen et al. (2003), the approach has the advantage to be applied in large-scale calculations in which the nature of irregular waves and the evolution of a wave spectrum and the processes of energy generation, dissipating and wave–wave interactions are included. The present phase-decoupled model does not take into account the changes in the Doppler-shift of the effective wavenumber and the wave direction as addressed in Liu (1990). The model is limited for the case that the ambient current strength has the same order with the wave speed, i.e. $U_s/c=1$.

Acknowledgements

This research was supported by the National Science Council under grant number NSC95-2623-7-006-006-D, Taiwan, and in part by the Research Center of Ocean Environment, National Cheng Kung University, Taiwan.

Appendix A

The EMSE (Extend Mild-Slope Equation) is given as

$$\begin{aligned}\nabla_h\cdot\left(cc_g\nabla_h\phi\right)+k^2cc_g\phi+\left(f_1g\nabla_h^2h+f_2gk|\nabla_hh|^2\right)\phi\\+i\omega[\boldsymbol{U}\cdot\nabla_h\phi+\nabla_h\cdot(\boldsymbol{U}\phi)]-\left(\sigma^2-\omega^2\right)\phi\\=\nabla_h\cdot[\boldsymbol{U}(\boldsymbol{U}\cdot\nabla_h\phi)]\end{aligned}\tag{A.1}$$

and the velocity potential is defined as

$$\phi(x,y)=\frac{iga}{\sigma}\frac{\cosh k(z+h)}{\cosh kh}e^{iS(x,y)}\tag{A.2}$$

Substituting Eq. (A.2) into Eq. (A.1) yields a complex equation, such that

$$\begin{aligned}
&\left[\nabla_h\left(cc_g\nabla_h a\right)-cc_g a|\nabla_h S|\right]e^{iS}\\
&+i\left(a\nabla_h cc_g\cdot\nabla_h S+2cc_g\nabla_h a\cdot\nabla_h S+acc_g\nabla_h^2 S\right)e^{iS}\\
&+\left[k^2cc_g-\left(\sigma^2-\omega^2\right)+f_1g\nabla_h^2h+f_2gk|\nabla_h h|^2\right]ae^{iS}\\
&+\left\{\nabla_h\cdot[\mathbf{U}(\mathbf{U}\cdot\nabla_h a)]-\nabla_h S\cdot[\mathbf{U}(a\mathbf{U}\cdot\nabla_h S]\right\}e^{iS}\\
&+i\left\{\nabla_h S\cdot[\mathbf{U}(\mathbf{U}\cdot\nabla_h a]+\nabla_h[\mathbf{U}(a\mathbf{U}\cdot\nabla_h S)]\right\}e^{iS}=0
\end{aligned}\tag{A.3}$$

and the real part of Eq. (A.3) is written as

$$\begin{aligned}
&\nabla_h\cdot\left(cc_g\nabla_h a\right)+\left(k^2-|\nabla_h S|^2\right)cc_g a+\left(f_1g\nabla_h^2h+f_2gk|\nabla_h h|^2\right)a\\
&+\left[-\sigma^2+(\omega-\boldsymbol{U}\cdot\nabla_h S)^2\right]a\\
&=\nabla_h\cdot[\boldsymbol{U}(\boldsymbol{U}\cdot\nabla_h a)].
\end{aligned}\tag{A.4}$$

The wavenumber K is defined as $K=\nabla_h S$ where S denotes the scalar phase function. Eq. (A.4) can thus be rewritten as

$$\begin{aligned}
K^2&=|\nabla_h S|^2\\
&=k^2+\frac{\nabla_h\cdot\left(cc_g\nabla_h a\right)}{cc_g a}+\frac{f_1g\nabla_h^2h+f_2gk|\nabla_h h|^2}{cc_g}\\
&\quad+\frac{1}{cc_g}\left\{-\sigma^2+(\omega-\boldsymbol{U}\cdot\nabla_h S)^2-\frac{1}{a}\nabla_h\cdot[\boldsymbol{U}(\boldsymbol{U}\cdot\nabla_h a)]\right\}
\end{aligned}\tag{A.5}$$

References

Ardhuin, F., Herbers, T.H.C., 2002. Bragg scattering of random surface gravity waves by irregular seabed topography. Journal of Fluid Mechanics 451, 1–33.

Arthur, R.S., 1950. Refraction of shallow water waves: the combined effects of currents and underwater topography. EOS Transaction AGU 31, 549–552.

Berkhoff, J.C.W., 1972. Computations of combined refraction, diffraction and reflection. Proceedings of the 13th International Conference on Coastal Engineering. ASCE, New York, pp. 471–490.

Booij, N., Holthuijsen, L.H., Doorn, N., Kieftenburg, A.T.M.M., 1997. Diffraction in a spectral wave model. Proceedings of the 3rd International Symposium on Ocean Wave Measurement and Analysis, WAVES' 97. ASCE, New York, pp. 243–255.

Booij, N., Ris, R.C., Holthuijsen, L.H., 1999. A third generation wave model for coastal regions: part I. Model description and validation. Journal of Geophysical Research 104 (C4), 7649–7666.

Chamberlain, P.G., Porter, D., 1995a. The modified mild-slope equation. Journal of Fluid Mechanics 291, 393–407.

Chamberlain, P.G., Porter, D., 1995b. Decomposition methods for wave scattering by topography with application to ripple beds. Wave Motion 22, 201–214.

Chandrasekera, C.N., Cheung, K.F., 1997. Extended linear refraction–diffraction model. Journal of Waterway, Port, Coastal and Ocean Engineering 123, 280–286.

Davies, A.G., Heathershwa, A.D., 1984. Surface propagation over sinusoidally varying topography. Journal of Fluid Mechanics 144, 419–446.

Dingemans, M.W., 1985. Surface wave propagation over an uneven bottom; evaluation of two-dimensional horizatal wave model. Report W301. Delft Hydraulics. 117 pp.

Fuhrman, D.R., Madsen, P.A., 2009. Tsunami generation, propagation, and run-up with a hiher order Boussinesq model. Coastal Engineering 56 (7), 747–758.

Gobbi, M.F., Kirby, J.T., Wei, G., 2000. A fully nonlinear Boussinesq model for surface waves. II. Extension to $O((kh)^4)$. Journal of Fluid Mechanics 405, 182–210.

Goda, Y., 1999. A comparative review on the functional forms of directional wave spectrum. Coastal Engineering Journal 41 (1), 1–20.

Hasselmann, K., Barnett, T.P., Bouws, E., Carlson, H., Cartwright, D.E., Enke, K., Ewing, J.A., Gienapp, H., Hasselmann, D.E., Kruseman, P., Meerburg, A., Müller, P., Olbers, D.J., Richter, K., Sell, W., Walden, H., 1973. Measurement of wind–wave growth and swell decay during the Joint North Sea Wave Project (JONSWAP). Ergnzungsheft zur Deutschen, Hydrographischen Zeitschrift 8 (12), 95.

Holthuijsen, L.H., 2007. Waves in oceanic and coastal waters. Cambridge University Press. 440 pp.

Holthuijsen, L.H., Herman, A., Booij, N., 2003. Phase-decoupled refraction–diffraction for spectral wave models. Coastal Engineering 49, 291–305.

Hsu, T.W., Wen, C.C., 2001a. A parabolic equation extended to account for rapidly varying topography. Ocean Engineering 28, 1479–1498.

Hsu, T.W., Wen, C.C., 2001b. On radiation boundary conditions and wave transformation across the surfzone. China Ocean Engineering 15 (3), 395–406.

Hsu, T.W., Ou, S.H., Liau, J.M., 2005. Hindcasting nearshore wind waves using a FEM code for SWAN. Coastal Engineering 52, 177–195.

Ilic, S., van der Westhuysen, A.J., Roelvink, J.A., Chadwick, A.J., 2007. Multidirectional wave transformation around detached breakwaters. Coastal Engineering 54, 775–789.

Isobe, J.T., 1987. A parabolic equation model for transformation of irregular waves due to refraction, diffraction and breaking. Coastal Engineering. Japan 30, 33–47.

Janssen, P.A.E.M., Hasselmann, K., Hasselmann, S., 1994. The kinematic part of the energy balance equation. In: Komen, et al. (Ed.), Dynamics and Modelling of Ocean Waves. Cambridge University Press, pp. 207–215.

Kirby, J.T., 1984. A note on linear surface wave–current interaction. Journal of Geophysical Research 89 (C1), 745–747.

Kirby, J.T., 1986. Higher-order approximation in the parabolic equation method for water waves. Journal of Geophysical Research 91 (C1), 933–952.

Lee, C., Park, W.S., Cho, Y.S., Suh, K.D., 1998. Hyperbolic mild-slope equations extended to account for rapidly varying topography. Coastal Engineering 34, 243–257.

Liu, P.L.-F., 1983. Wave–current interactions on a slowly varying topography. Journal of Geophysical Research 88 (C7), 4421–4426.

Liu, P.L.-F., 1990. Wave transformation. The Sea: Ocean Engineering Science, 9, pp. 27–63.

Lynett, P.J., Wu, T.R., Liu, P.L.F., 2002. Modeling wave runup with depth-integrated equations. Coastal Engineering 46 (2), 89–107.

Madsen, P.A., Sørensen, O.R., 1992. A new form of the Boussinesq equations with improved linear dispersion characteristics: part 2, A slowly-varying bathymetry. Coastal Engineering 18, 183–205.

Madsen, P.A., Bingham, H.B., Schäffer, H.A., 2003. Boussinesq-type formulation for fully nonlinear and extremely dispersive water waves: derivation and analysis. Proceedings. Royal Society of London A459, 1075–1104.

Marcos, F., 2003. Logiciel TOMAWAC de Propagation de Houle En Elements Finis. Notice D'utilisation. Version 5.2. EDF Département Laboratoire National d'Hydrauliqueet Environnement, Chatou, France. 180 pp.

Mase, H., 2001. Multi-directional random wave transformation model based on energy balance equation. Coastal Engineering Journal 43 (4), 317–337.

Massel, S.R., 1993. Extended refraction–diffraction equation for surface waves. Coastal Engineering 19, 97–126.

Nwogu, O., 1993. An alternative form of the Bonssineq equations for modeling the propagation of waves from deep water to shallow water. Journal of Waterway, Port, Coastal and Ocean Engineering 119 (6), 618–638 ASCE.

Peregrine, D.H., 1967. Long waves on a beach. Journal of Fluid Mechanics 27 (4), 815–827.

Resio, D.T., 1988. A steady-state wave model for coastal applications. Proceedings 21st International Conference on Coastal Engineering. ASCE, New York, pp. 929–940.

Ris, R.C., Holthuijsen, L.H., Booij, N., 1999. A third-generation wave model for coastal regions: part 2, verification. Journal of Geophysical Research 104 (C4), 7667–7682.

Rivero, F.J., Arcilla, A.S., Carci, E., 1997. Analysis of diffraction in spectral wave models. Proceedings of the 3rd International Symposium on Ocean Wave Measurement and Analysis, WAVES '97. ASCE, New York, pp. 431–445.

Smith, J.M., Sherlock, A.R., Resio, D.T., 2001. STWAVE: Steady-State Spectral Wave Model User's Manual for STWAVE, Version 3.0. Coastal and Hydraulics Laboratory, US Army Corps of Engineers. 80 pp.

Tsai, C.P., Chen, H.B., Hsu, J.R.C., 2001. Calculations of wave transformation across the surf zone. Ocean Engineering 28, 941–955.

Vincent, C.L., Briggs, M.J., 1989. Refraction–diffraction of irregular waves over a mound. Journal of Waterway, Port, Coastal and Ocean Engineering 115 (2), 269–284 ASCE.

Wei, G., Kirby, J.T., Grilli, S.T., 1995. A fully nonlinear Boussinesq model for surface waves, part 1. Highly nonlinear unsteady waves. Journal of Fluid Mechanics 294, 71–92.

Zelt, J.A., 1991. The runup of nonbreaking and breaking solitary waves. Coastal Engineering 15 (3), 205–243.